Test Bench and Frequency Response of a Magnetic Antenna used in GIS PD Measurements

Mier Escurra, Christian; Mor, Armando Rodrigo

DOI
10.1109/EIC49891.2021.9612372

Publication date
2021

Document Version
Accepted author manuscript

Published in
2021 IEEE Electrical Insulation Conference (EIC)

Test Bench and Frequency Response of a Magnetic Antenna used in GIS PD Measurements

Christian Mier Escurra
DC Systems, Energy Coversion & Storage
Delft University of Technology
Delft, Netherlands
C.MierEscurra@tudelft.nl

Armando Rodrigo Mor
Instituto de Tecnología Eléctrica
Universitat Politècnica de València
Valencia, Spain
arrodmor@upvnet.upv.es

***Abstract*— Gas insulated substations (GIS) have increased in the electric power system in recent years and is expected to continue increasing in the following years. The GIS has remarkable advantages over air insulated substation in offshore windfarms where the installation space is limited. The outlying location of the GIS demands a robust monitoring system. It is well known from literature that partial discharge (PD) measurements are an accepted method for insulation diagnosis and in many cases a required part of the acceptance protocol for many high voltage (HV) assets. In a recent investigation, a new concept of PD measurements in GIS using a Very High Frequency (VHF) Sensor (so-called Magnetic Antenna) has been demonstrated. Unlike Ultra High Frequency (UHF) technology, the presented PD sensor has a sensitivity better than 5 pC and yield an estimation of the charge magnitude, thus providing information about the severity of the insulation degradation. In this paper, a test bench for the characterization of the magnetic antenna is proposed. The magnetic antenna and a traditional UHF antenna are tested in the frequency domain up to 1 GHz, and in the time domain using different wave-shapes. Additionally, using the test bench, it is demonstrated the homogeneity of the PD current propagating in the GIS in the transverse electromagnetic (TEM) mode. The charge is estimated using the double integral voltage method, showing low errors. The results from the research gives a preface for further investigation in the design of the magnetic antenna.**

Keywords—Partial discharge, VHF, UHF, gas insulated substation, magnetic antenna, loop antenna, test bench, frequency response.

I. INTRODUCTION

The use of gas insulated substations (GIS) have been growing in the last years for several reasons: the GIS highlight easier installation and operation, long life span, low maintenance and increased reliability compared to air insulation substations (AIS). The last two are of high importance for outlying locations: offshore windfarms for instance. According to [1], it is expected that the GIS market will be valued $41,059.8 USD millions by 2025 as compared to the $15,416.1 USD millions in 2016.

The main drawback in a GIS is the high cost over an AIS, therefore, it is critically important the monitoring of the system to prevent failures. As mentioned before, the main application is in confined areas such as an offshore platform, featuring the importance of a remote monitoring. It is well known from literature that partial discharge (PD) measurements are an accepted method for insulation diagnosis [2].

One of the many physical phenomena produced by a PD is the propagation of electromagnetic (EM) waves. The GIS acts as a coaxial waveguide with three propagation modes: transverse electromagnetic (TEM), transverse electric (TE) and transverse magnetic (TM). The TE and TM have a cutoff frequency which depends on the geometry of the cross-section of the GIS. In (1) the cut-off frequency of the first high-order TE mode is presented, where *c* represents de speed of light, ε_r is the relative permittivity of the dielectric and r_i and r_o correspond to the inner and outer radii of the electrodes, respectively.

$$f_0 = \frac{c}{\pi\sqrt{\epsilon_r}(r_i + r_{0)}} \quad (1)$$

It has been discussed in previous investigations that is not possible to extract the charge magnitude from ultra-high frequency (UHF) signals in a GIS, [2] and [3]. Additionally, in [4], it is demonstrated that the charge information is found in the low frequency range of the PD pulse. Therefore, a measuring system operating solely in the TEM mode must be used for the purpose of charge estimation [5].

Previous investigations found that the magnetic field produced by the PD current can be sensed in the TEM mode with a magnetic antenna (MA), making it possible to estimate the charge magnitude with an error around 30%, and sensitivity below 5 pC ([6] and [7]).

In this paper, a matched broad bandwidth test bench up to 1 GHz is used for full characterization of the magnetic antenna in the VHF and UHF ranges. It is believed that with the contribution presented in this paper, an extended design of the MA can be achieved, improving the sensitivity and charge estimation accuracy.

II. TEST BENCH

To measure the frequency response of the antenna, the output and input signal is compared in the desired frequency ranges. For that purpose, the vector network analyzer (VNA) ROHDE&SCHWARS ZVB4 (300KHz-4GHz) was used. The VNA has an input and output impedance of 50 Ω, therefore the characteristic impedance through the whole test bench must be maintained at the same value for proper matching.

To avoid reflections in the measuring circuit the GIS used for the test bench is matched at 50 Ω. Considering the GIS as a coaxial line, the relation between the outer and inner conductors (r_o and r_i) in (2) must be 2.3:1.

"This project 19ENG02 FutureEnergy has received funding from the EMPIR programme cofinanced by the Participating States and from the European Union's Horizon 2020 research and innovation programme"

$$Z_0 = \sqrt{\frac{\mu}{\varepsilon}} \frac{ln(r_o/r_i)}{2\pi} \quad (2)$$

The signal is transmitted from the VNA to the GIS by means of a N-type connector. The N-type connector has a small diameter in comparison with the GIS's diameter, thus a smooth transition must be implemented between them. A transition cone is used for this purpose, which grows from the diameter of the N-type connector to the diameter of the GIS. The smoothness of the transition depends on the length of the cones, where a large cone gives a better transition. If the slope of the cone is too steep, then reflections occur.

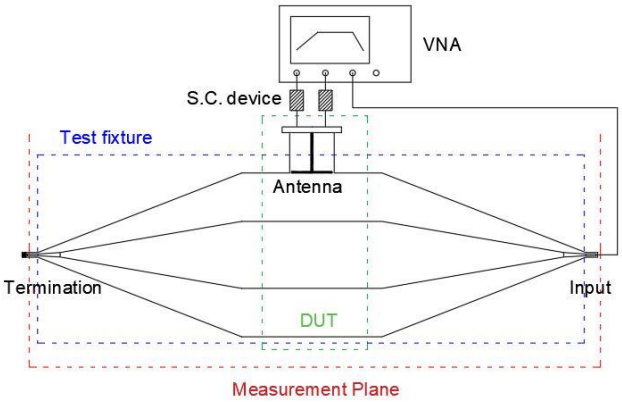

Fig. 2. Diagram of the test bench

To have a real representation of the interaction between the antennas and the GIS, a real GIS enclosure 360 mm in length and 415 mm in diameter was used.

The transition cones were handcrafted in a workshop: the


Fig. 1. Photo of the test bench

inner cylindrical and conical conductor were made of paperboard covered with aluminum foil, giving it a light weight to be solely supported by the inner pin of the N-type connector. The outer cone was hand rolled using a 1 mm thickness aluminum sheet and an aluminum flange was welded in the base and vertex of the cones. The result can be seen in Fig. 1. and Fig. 2.

Using a cone with 520 mm length, the frequency response up to 1 GHz is presented in Fig. 3, where the transmission parameter (S21) is below -1dB. It has been discussed in [2] - [5] that the charge magnitude estimation is possible only in the TEM mode, hence, the MA's PD measuring system BW is limited up to the cutoff frequency of the TE mode calculated using (1), for instance, using the dimensions of the 400 kV GIS located in the laboratory of Delft University of Technology, the TE cutoff frequency is about 284 MHz, thus, the test bench frequency range covers the BW of the MA.

The calibration of the VNA is performed using a calibration unit. The GIS-compartment, cones, and antenna are considered as the "measurement plane" (Fig. 2). The "DUT" (device under test) is the antenna and its interaction with the surroundings (enclosure and inner conductor) leaving the GIS-compartment and cones as part of the DUT but also as the "test fixture", therefore, it is impossible to de-embed just the test fixture. As shown in Fig 3, the attenuation due to the test fixture is low in the 0-1GHz range, just the time delay must be corrected due to the electric length, for that (3) is used, where: l is the length between vertices, c is the speed of light in vacuum, f is the frequency and ϕ is the phase delay.

$$\varphi = 2\pi f \sqrt{\epsilon} \frac{l}{c} \quad (3)$$

In Fig. 3, the phase without and with correction is shown in red and blue, respectively. Note that once the antenna is measured, the electric length used for the phase correction is half the test fixture. For additional devices with considerable electric length such as filters and amplifiers, the phase delay must be corrected as well.

III. Antenna's Frequency Response Measurement

For this investigation three different antennas were measured and compared: an UHF disk antenna, a MA with shield and a MA without shield. The unshielded antenna is constructed in a PCB plate and the shielded antenna is built using a RG174A-U coaxial cable. The un-shielded MA consist of a loop, where the terminals are connected to the inner and outer conductor of the feeder coaxial cable (Fig. 4). The shielded MA consist of a shielded loop, the inner conductor of the end of the loop is connected to the shield of the feeder coaxial cable, and the end of the outer conductor is left open circuited (Fig. 5). For both antennas, the shield of the feeder coaxial cable is grounded to the GIS enclosure. A detailed explanation of the shielded antenna is given in [6].

The test set-up used for the frequency response measurement is presented in Fig. 2. One of the cone's termination is connected to the VNA input, the other one to a 50 Ω termination. The

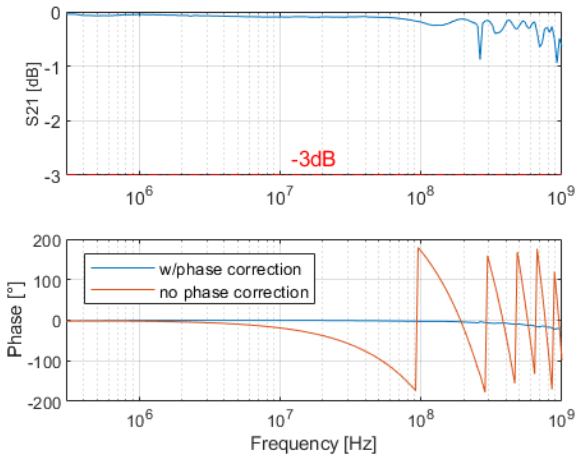

Fig. 3. Test bench frequency response amplitude and phase.

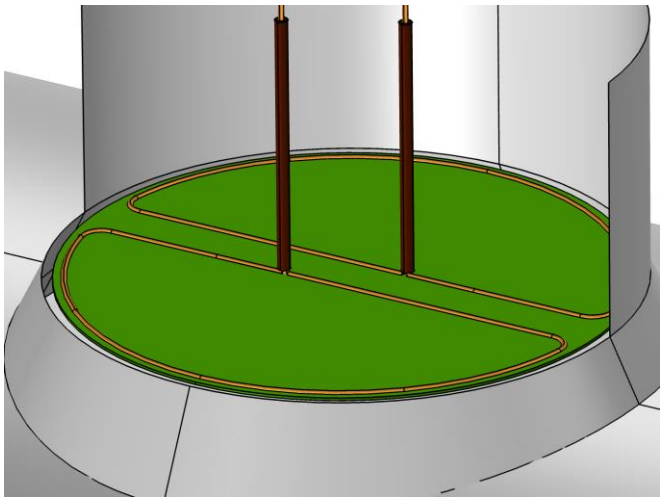

Fig. 4. CAD drawing of the unshielded MA.

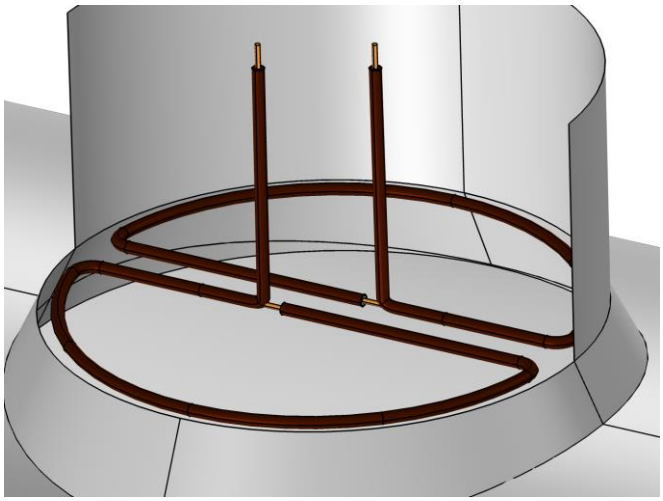

Fig. 5. CAD drawing of the shielded MA.

output of the antennas can be connected directly to the VNA port or through a signal conditioning (S.C.) device such as an amplifier and/or a filter.

A comparison of the magnitude of the three antennas is presented Fig. 6. The three types of antennas show a slope in the low frequency range due to their derivative components: for the MAs is the mutual inductance between the antenna's mounting hole and the antenna [7], for the UHF coupler is the mutual capacitance between the GIS's inner conductor and the antenna

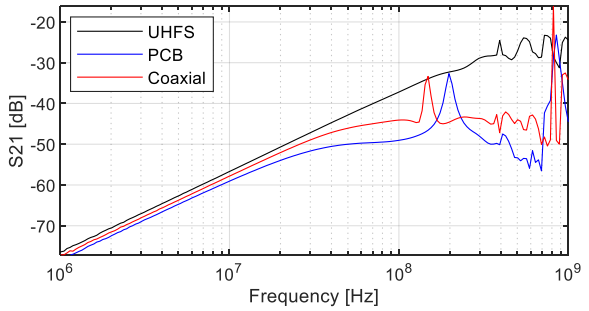

Fig. 6. Antenna's frequency response

[8]. After some tens of MHz, the loop antennas reach a flat area influenced by the self-inductance of the loop and the load impedance. For the shielded and unshielded magnetic antennas, a resonance appears at 150MHz and 200MHz, respectively: although this resonance will amplify the signal it also distorts the shape of the measured pulse.

In [9], it is stated that by using symmetric loops; each of them in each half of the antenna's mounting hole, it is possible to discriminate the interference from the PD signal. Fig. 7 shows the measurement of the two loops, the amplitude and phase between them is almost the same up to a certain frequency, confirming the theory. At the resonance frequency the phase between the loops is the same, concluding that the resonance comes from a common mode signal and that is not inherent of the antenna.

IV. Antenna's Time Domain Measurement

To measure the signals in the time domain, the test-setup showed in Fig. 8 was arranged. This time, several input signals and an oscilloscope were used to record the injected and measured signals. To have a better visualization in the following plots, an intentional delay between signals was introduced. All the measurements were performed using voltage amplifiers for signal conditioning.

In Fig 9. the output voltage of the UHF antenna and shielded MA is shown, an UHF pulse with a bandwidth DC - 750MHZ was injected: the MA signal is heavily distorted by the resonances in 150 MHz and 800 MHz.

In Fig. 10, the signal is conditioned using a 270 MHz and 100 MHZ low pass filters for the UHF sensor and the MA, respectively. The MA exhibit a clear derivative response of the rise and fall time, however, because of the short BW, the pulse has a longer duration making it prone to have overlapping of reflected pulses in a real GIS. The BW of the filter must be properly analyzed to produce a signal with enough sensitivity

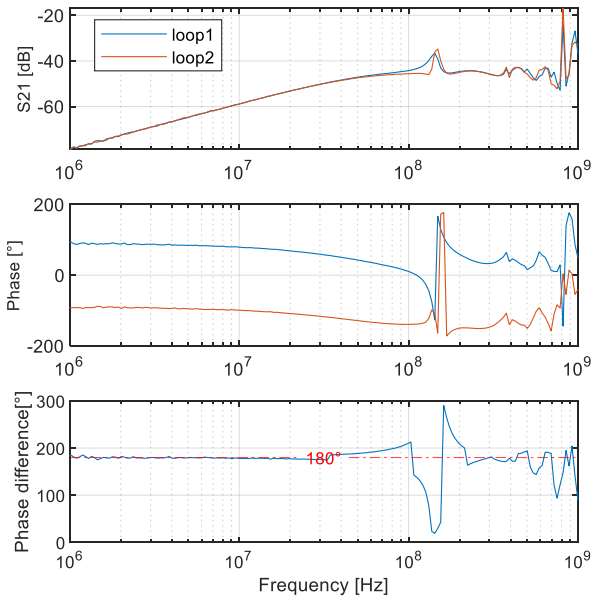

Fig. 7. Frequency response of loops in the MA.

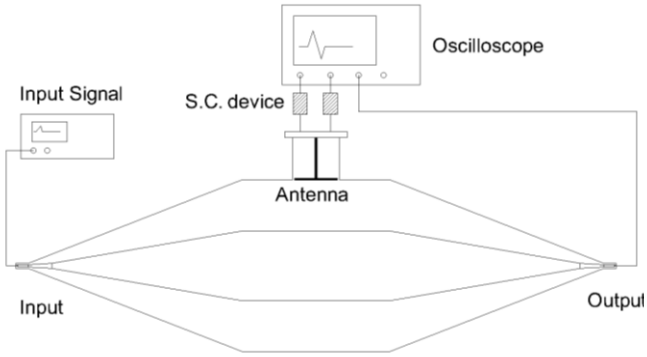

Fig. 8. Time domain test-setup.

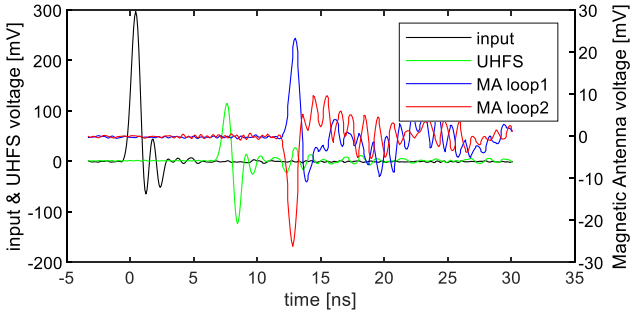

Fig. 9. Time domain measurement of antennas with a UHF pulse.

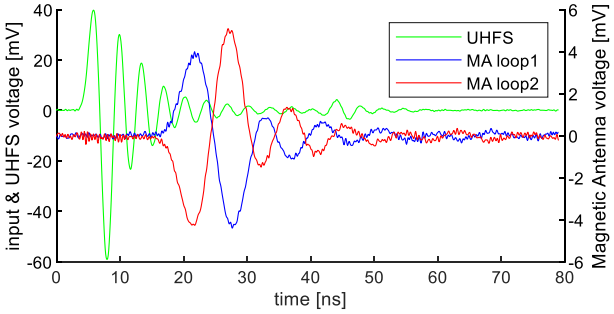

Fig. 10. Time domain measurement of antennas using filters with an injected UHF pulse.

and spatial resolution. Additionally, by filtering the resonance in the MA, the symmetry between the output signals of the two loops is appreciated.

Using the double integral voltage method presented in [10], Table 1 shows charge estimation error for some input signals. As expected, the charge estimation error is big when the resonance is not filtered.

Table 1. Charge estimation with different injected pulses.

	|Error|	
Input signal	***UHFS***	***MA***
1GHz Pulse no filters	11.3%	42.4%
1GHz Pulse w/filters	6.5%	10.1%
45MHz Pulse w/filters	2.4%	2.2%
4.5MHz Pulse no filters	4.1%	2.3%
Gaussian pulse sigma=21.2ns	3.3%	2.4%
IEC 60270 Calibration 1nC	6.2%	5.2%

V. Conclusions

This work shows a handcrafted test bench for measuring the frequency and time domain response of antennas used in online PD measurements in GIS. The test bench is designed for electromagnetic waves in the TEM mode, covering a frequency range up to 1GHz.

Frequency domain measurements were done connecting a VNA to the test bench. Three antennas were tested in the frequency domain: a UHF antenna, a shielded MA and an unshielded MA. To fully understand the MA's behavior, it is important to extend the mathematical model presented in [7] to higher frequencies. It has been demonstrated that the TEM mode propagation is distributed uniformly in the antenna's mounting hole, inducing a symmetric signal between the two loops of the MA. This symmetry helps to distinguish a real PD from noise.

Measurements in the time domain shows an oscillating output in the MA due to the resonances in the frequency domain. To mitigate the oscillations a lowpass filter was used. The antenna's design and signal conditioning devices must be properly analyzed to produce a signal with enough sensitivity and resolution.

References

[1] The Insight Partners, «ASD Reports,» November 2017. [On line]. Available: https://www.asdreports.com/market-research-report-432404/gas-insulated-substation-market-global-analysis-forecasts. [Último acceso: 20 October 2020].

[2] Working Group D1.33, «Guidelines for unconventional Partial Discharge Measurements,» Cigre, vol. D1, nº 444, p. 58, 2010.

[3] G. Behrmann y Z. Tanasoc, «UHF PD signal transmission in GIS: Effects of 90 bends and L-shaped CIGRE step 1 test section.,» p. 9, 2019.

[4] A. Rodrigo, P. Morshuis y J. Smit, «Comparison of Charge Estimation Methods in Partial Discharge Cable Measurements,» IEEE Transactions on Dielectrics and Electrical Insulation., vol. 22, nº 2, p. 8, 2015.

[5] S. Ohtsuka y T. Teshima, «Relationship between PD-induced electromagnetic wave measured with UHF emthod and charge quantity obtained by PD current waveform in model GIS,» de Annual Report Conference on Electrical insulation and Dielectric Phenomena, Kansas City, 2007.

[6] A. Rodrigo, F. A. Muñoz y L. C. Castro, «A Novel Antenna for Partial Discharge Measurements in GIS Based on Magnetic Field Detection,» Sensors, vol. 19, nº 858, p. 17, 2018.

[7] A. Rodrigo, L. C. Castro y F. A. Muñoz, «A magnetic loop antenna for partial discharge measurements on GIS,» Elsevier International Journal of Electrical Power & Energy Systems, vol. 115, nº 105514, p. 6, 2019.

[8] R. Kurrer, Teilentladungsmessung im Gigaherts-Frequencbereich an SF6-isolierten Schaltanlagen, Stuttgart, 1997.

[9] F. Muñoz y R. Armando, «Partial discharges and noise discrimination using magnetic antennas, the cross wavelet transform and support vector machines.,» Sensors, p. 14, 2020.

[10] A. Rodrigo, F. Muñoz y C. C. Luis, «Principles of Charge Estimation Methods Using High'Frequency Current Transformers Sensors in Partial Discharge Measurements,» Sensors, vol. 20, nº 2520, p. 16, 2020.